# Experimental Demonstration of Surface Acoustic Wave Propagation on $\alpha$-$GeO_2$ for Wireless, Passive Sensor Design

W. Daniau, R. Salut, J.-M Friedt
*FEMTO-ST, UFC/CNRS 6174*
Besançon, France
jmfriedt@femto-st.fr

A. Peña, J. Debray, B. Menaert
*Institut Néel CNRS/UGA 2940*
Grenoble, France

P. Armand, P. Papet
*ICGM UMR5253*
Montpellier, France

A. Penarier, P. Nouvel
*IES UMR5214*
Montpellier, France

***Abstract*—On the path towards developing passive transducers for wireless sensing in high temperature (>560°C) environments, we experimentally demonstrate the design, manufacturing and wireless interrogation of resonators patterned on $GeO_2$ substrates, leading to an initial estimate of the coefficients of temperature with frequency of surface acoustic waves propagated on this substrate.**

***Index Terms*—$GeO_2$, surface acoustic wave, resonator, passive wireless sensor**

## I. Introduction

Passive sensors using the linearity of piezoelectric effects for far-field wireless cooperative target short range RADAR measurement have been investigated for probing quantities in environments incompatible with a wired connection, whether moving targets or harsh environmental conditions. High temperature monitoring matches the latter context, with most investigations focusing on langasite family materials concluding to the long-term instability of this subtrate when exposed to high temperature. In this investigation, a material of the same crystal class (point group 32) as $\alpha$-quartz and without phase transition up to its melting temperature (1116°C) – $\alpha$-$GeO_2$ – is considered as the substrate for designing and realizing a passive transducer compatible with short range RADAR interrogation.

## II. $\alpha$-$GeO_2$ material

The oriented substrates used in this work have been obtained from centrimetric size $\alpha$-$GeO_2$ bulk single crystals grown by the Top Seeded Solution Growth–Slow Cooling (TSSG-SC) technique [1]. Although two different chemical systems, $GeO_2$–$K_2Mo_4O_{13}$ and $GeO_2$–$K_2Mo_4O_{13}$—$K_6P_4O_{13}$, allow to grow $\alpha$-$GeO_2$ crystals (Fig. 1) that do not show any phase transition up to the melting temperature, the crystal quality and the reproducibility of the growth process is improved while using the second one. Only a small evolution of the piezoelectric constants and dielectric properties up to 600°C have been observed, making these $\alpha$-$GeO_2$ crystals potential good candidates to be used in harsh conditions and high temperature environments [2].

This work is supported by the French National Research Agency ANR under the OVERHEAT grant 21-CE08-0017. The RENATECH network is acknowledged for supporting the MIMENTO cleanroom facility.

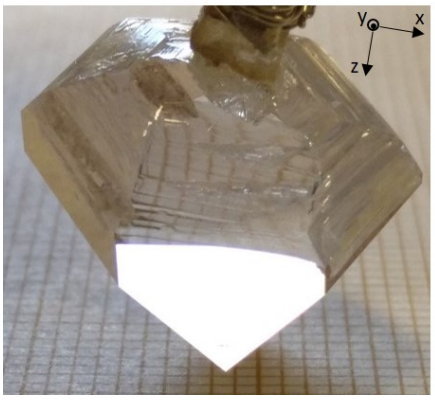


Fig. 1. $\alpha$-$GeO_2$ crystal as grown prior to dicing slides used for patterning electrodes for propagating SAW. The underlying grid spacing is 1 mm so each crystal side is about 2 cm.

## III. Surface Acoustic Wave propagation: simulation

The propagation of Surface Acoustic Waves has been investigated numerically previously [3]. In this work, the mechanical and electrical constants extracted from [4] are used to define the mixed matrix acoustic wave propagation and reflection parameters [5]. Based on this analysis, and considering at first aluminum electrodes selected for their adequation to cleanroom manufacturing technologies for repeating multiple prototyping steps on a given substrate, the electromechanical coupling coefficient map, acoustic velocity map, and beam steering map are computed.

The electromechanical coupling coefficient $K^2$ is observed (Fig. 2) to remain below the 1% range, with a maximum at $l = t = 0$ in the IEEE Stds 176-1949 orientation standards. For this propagation direction, the velocity is slowest around 2100 m/s (Fig. 3), leading to lithography resolution challenges when designing Ultra-High Frequency (UHF) range transducers, e.g. meeting the radiofrequency emission regulations in

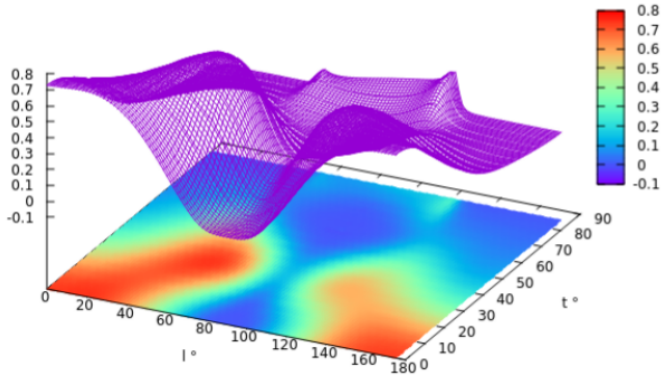


Fig. 2. Electromechanical coupling coefficient (%) of Rayleigh waves for $\alpha$-$GeO_2$ $(YXlt)/l/t$ as a function of cut angle $l$ and propagation angle $t$.

the narrowband European Industrial, Scientific and Medical (ISM) band centered on 434 MHz.

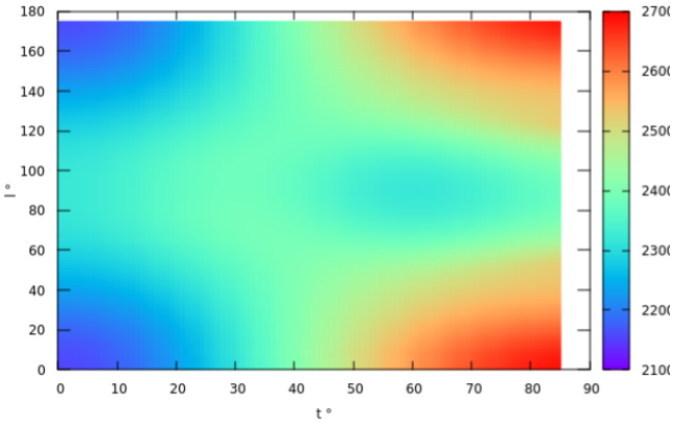


Fig. 3. Velocity map (m/s) of Rayleigh waves for $\alpha$-$GeO_2$ $(YXlt)/l/t$ as a function of cut angle $l$ and propagation angle $t$.

The beamsteering is negligible in this propagation direction (Fig 4), easing the design of a resonator, the only geometry compatible with delaying the transducer response beyond clutter for a wireless interrogation using a short range RADAR system.

From this acoustic propagation modelling, the $(YX)$ cut of $\alpha$-$GeO_2$ is selected for manufacturing tranducers.

## IV. Transducer Design and Manufacturing

From the previous analysis, the low electromechanical coupling coefficient prevents the design of a reflective delay line, and a single port resonator architecture has been selected with 78 interdigitated electrode pairs in the transducer and 80 electrodes in the Bragg mirrors on each side in either synchronous and asynchronous designs, aimed at maximizing the quality factor $Q$ at resonance frequency $f$. Indeed the objective of separating the sensor response decaying as $Q/(\pi f)$ from clutter is to reach a $Q$-factor high enough for clutter to have faded out, with an objective in the $Q \simeq 5000$ optimum between sensor identification and measurement speed to reach

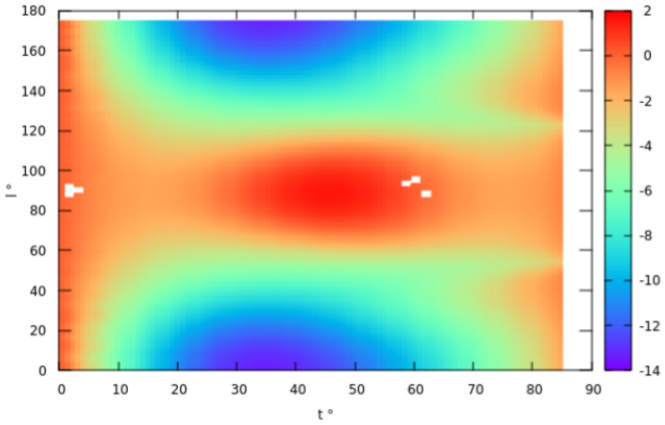


Fig. 4. Beam steering map (°) of Rayleigh waves for $\alpha$-$GeO_2$ $(YXlt)/l/t$ as a function of cut angle $l$ and propagation angle $t$.

$\tau \geq 3.5$ $\mu$s assuming a short-range RADAR distance detection limit of 150 m.

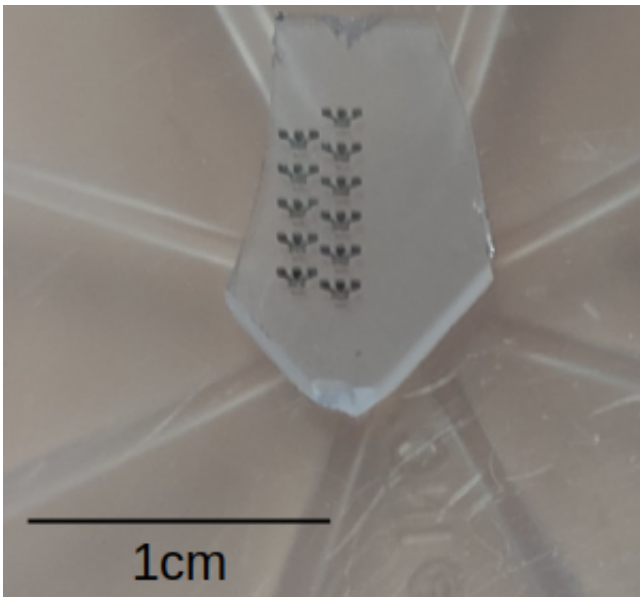


Fig. 5. $\alpha$-$GeO_2$ substrate patterned with aluminum electrodes using e-beam lithography.

Due to the minute dimensions of the available substrates (Fig. 5) and the challenges of patterning 1.15 $\mu$m-wide electrodes separated by 1.15 $\mu$m, electron-beam (e-beam) lithography, aluminum deposition by evaporation and lift-off techniques are employed to pattern interdigitated transducers. To be able to make several experiments, as only a single substrate sample was available, we had to recycle by etching the aluminum electrodes. Since this etching step uses a mix of acid, we observe a significant impact on the substrate leading to an increased roughness and even some bigger defects. Thus, only few patterning/etching cycles are possible before a new polishing of the substrate is needed.

Before being able to actually design a resonator suitable to

our needs, we have first patterned a set of basic resonator designs with varying wavelength $\lambda$ and metalization ratio to verify the accuracy of the model and be able to retrofit the mixed matrix parameters. These first experiments have exhibited important differences between the model and the actual measurements, such as a predicted resonant frequency at 530.7 MHz when the actual device has been measured at 497.5 MHz, or a 6.2% deviation. This implies that more precise measurements of the material coefficients are needed to be able to directly use the calculated mixed matrix parameters to make a resonator design. For example, this resonant frequency is directly linked to the wave velocity which for this class of material propagating a Rayleigh wave will be mainly given by $C_{11}$ and $C_{12}$ in addition to the material density which is measured with sufficient accuracy. However, one can assume that the global tendencies that have been explored (Fig. 2, 3, 4, 10, 9) will remain globally the same with some shifting of some of the remaining parameters.

Nevertheless, despite these discrepancies, it has been possible to retrofit the model and obtain a measurement based set of mixed matrix parameters that has been used to design an actual resonator. However, due to substrate recycling and the resulting surface degradation mentioned above, only a small number of working points could be used for this retrofit, impacting the final result accuracy, still better than the original one.

A single port resonator was then designed to have a resonant frequency at 434 MHz and expecting a $Q$ factor at 3600. Eleven devices were actually patterned on the substrate. Fig. 6 exhibits the $S_{11}$ measurement of one of these resonators. As these were fabricated on the third recycling cycle, the surface was degraded and only four devices exhibited a usable response.

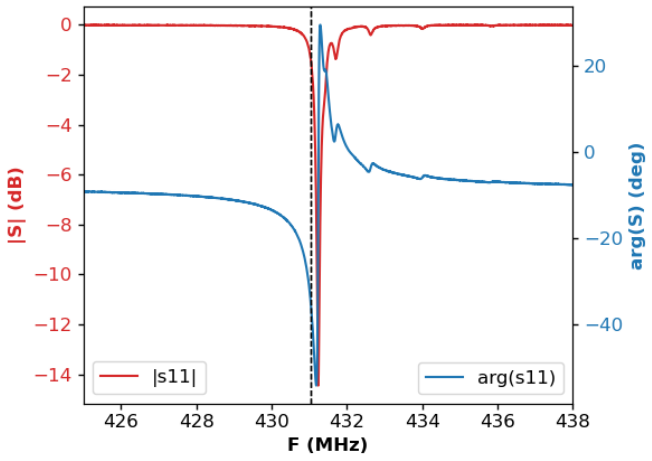


Fig. 6. $S_{11}$ measurement of the fabricated resonator

It exhibits a $Q$ factor equal to 2830 at a resonant frequency of 431.2 MHz. As mentioned earlier, due to the small number of working points that were used to construct our experimental mixed matrix parameters, we knew it will not be very accurate, but this is not so far to what was designed, the frequency shift is only 0.6%.

## V. Wireless Measurement

Multiple resonators with quality factors above 1000 were manufactured and characterized under a probe-station. The microwave probes were fitted with an helical monopole antenna and wireless interrogation in a sub-meter range was achieved using a dedicated short range RADAR system based on a frequency swept pulsed measurement for scanning the returned power as a function of frequency [6]. The interrogation range is at the moment limited by the quality factor of the resonator due to excessive degradation of the surface roughness after multiple processing steps (Fig. 7).

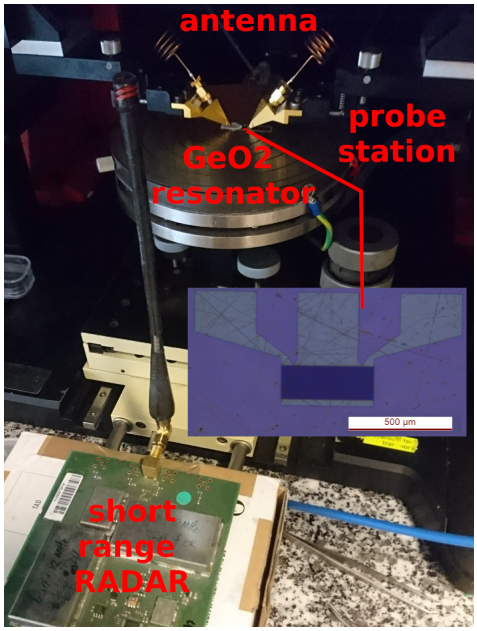


Fig. 7. Wireless sensing of the $GeO_2$ resonator shown in inset.

Nevertheless, multiple temperature sweeps were performed in the ambiant to 200°C temperature range, limited by the range accessible to the temperature controlled chuck, allowing for a first estimate of the first and second order Coefficient of Temperature with Frequency CTF (Fig. 8).

## VI. Wireless Passive High Temperature Sensor Design Consideration

Based on these preliminary results, multiple challenges remain to be tackled:

1) replacing aluminum electrodes with platinum electrodes induces the technological challenge of heavy mass loading of Pt with utmost sensitivity of the resonance frequency to metallization thickness – 3 MHz for 5 nm Pt thickness variation – and ratio,
2) antenna connection to the substrate since patterning antennas on the piezoelectric substrate has been demonstrated to be challenging [7], [8] and incompatible with the minute substrate dimensions for this new material,

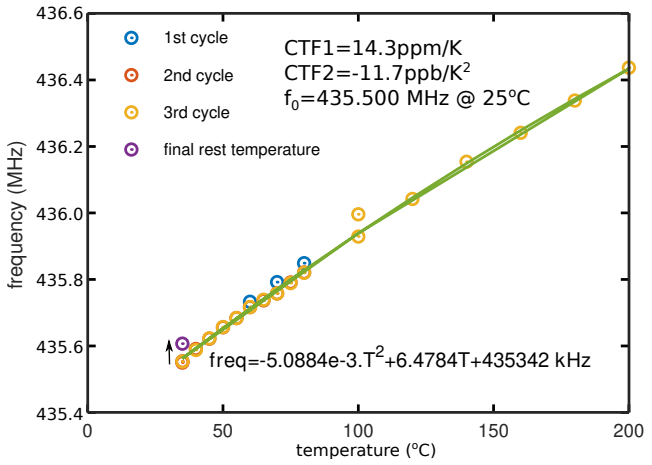


Fig. 8. Temperature dependence of the resonance frequency probed wirelessly by varying the substrate temperature through the heated chuck, and second order polynomial fit for extracting the first and second order coefficient of temperature with frequency.

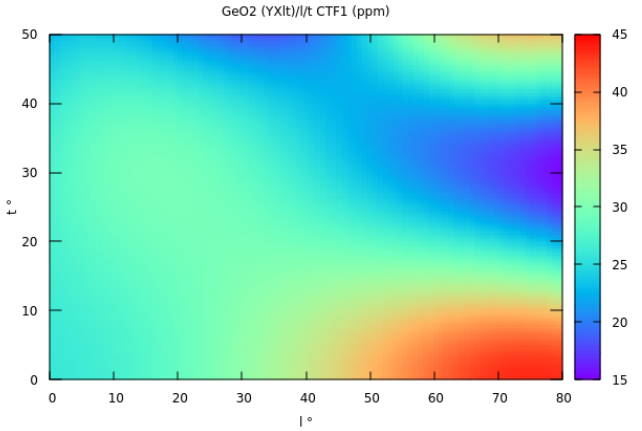


Fig. 9. Map of the first order coefficient of frequency with temperature $CTF_1$ of the $(YXlt)/l/t$ SAW propagation for $l \in [0:80]^\circ$ and $t \in [0:50]^\circ$ for which the electromechanical coupling coefficient is maximal.

3) tuning propagation direction adapted to temperature sensitivity so that either a subset of the whole temperature range is accessible within the 1.74 MHz-wide 434 MHz European ISM band, or the acoustic velocity and hence resonance frequency is insensitive enough to temperature to remain within this frequency range over the whole temperature range.

Indeed while an Oven-Controlled Crystal Oscillator (OCXO) is designed to operate at a fixed temperature under well defined conditions, a sensor is subject to widely varying environmental conditions, and predicting the temperature dependence of the acoustic velocity is a core design consideration when planning the frequency usage and meeting regulations. Furthermore, if the sensor is to provide a one-to-one relation between frequency and temperature, the turnover temperature must be outside the measurement range. Hence two simulations are performed based on material properties of the substrate for SAW device propagation: the first order coefficient of frequency with temperature $CTF_1$ (Fig. 9) and the turnover temperature (Fig. 10).

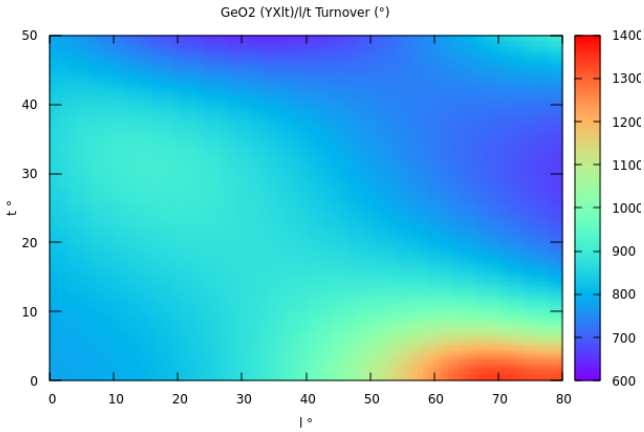


Fig. 10. Map of turnover temperature of the $(YXlt)/l/t$ SAW propagation for $l \in [0:80]^\circ$ and $t \in [0:50]^\circ$ for which the electromechanical coupling coefficient is maximal.

## VII. Conclusion

An experimental demonstration of surface acoustic wave propagation on $\alpha$-$GeO_2$ was achieved, allowing for wireless measurement of the passive transducer resonance frequency as a function of temperature at sub-meter range.

## References


[1] A. Lignie, B. Ménaert, P. Armand, A. Peña, J. Debray, and P. Papet, "Top seeded solution growth and structural characterizations of $\alpha$-Quartz-like structure $GeO_2$ single crystal," *Cryst. Growth. Des.*, vol. 13, no. 10, pp. 4220–4225, 2013.

[2] P. Papet, M. Bah, A. Haidoux, B. Ruffle, B. Ménaert, A. Peña, J. Debray, and P. Armand, "High temperature piezoelectric properties of flux-grown $\alpha$-$GeO_2$ single crystal," *J. Appl. Phys.*, vol. 126, no. 14, p. 144102, 2019.

[3] R. Taziev, "SAW properties in quartz-like $\alpha$-$GeO_2$ single crystal," in *Journal of Physics: Conference Series*, vol. 1015, no. 3. IOP Publishing, 2018, p. 032142.

[4] A. Lignie, P. Armand, and P. Papet, "Growth of piezoelectric water-free $GeO_2$ and $SiO_2$-substituted $GeO_2$ single-crystals," *Inorganic chemistry*, vol. 50, no. 19, pp. 9311–9317, 2011.

[5] S. Ballandras, A. Reinhardt, V. Laude, A. Soufyane, S. Camou, W. Daniau, T. Pastureaud, W. Steichen, R. Lardat, M. Solal *et al.*, "Simulations of surface acoustic wave devices built on stratified media using a mixed finite element/boundary integral formulation," *Journal of applied physics*, vol. 96, no. 12, pp. 7731–7741, 2004.

[6] J.-M. Friedt, C. Droit, G. Martin, and S. Ballandras, "A wireless interrogation system exploiting narrowband acoustic resonator for remote physical quantity measurement," *Rev. Sci. Instrum.*, vol. 81, p. 014701, 2010.

[7] M. Gallagher, B. Santos, and D. Malocha, "Wireless wideband SAW sensor – antenna design," in *IEEE International Frequency Control Symposium (IFCS)*, 2010, pp. 291–296.

[8] ——, "An integrated SAW sensor with direct write antenna," in *Joint European Frequency and Time Forum & IEEE International Frequency Control Symposium (EFTF/IFCS)*, 2013, pp. 450–453.